Tungsten erosion under combined hydrogen/helium high heat flux loading

H. Maier, H. Greuner, M. Balden, B. Böswirth, S. Elgeti, U. v. Toussaint, Ch. Linsmeier*

Max-Planck-Institut für Plasmaphysik, EURATOM Association, D-85748 Garching, Germany

*New address: Forschungszentrum Jülich GmbH, Institut für Energie- und Klimaforschung – Plasmaphysik, EURATOM Association, 52425 Jülich, Germany

Abstract

We investigated the erosion behaviour of tungsten under irradiation with a fusion reactor-relevant H/He mixture of 94%/6% at a power density of 10 MW/m². The investigated surface temperatures range up to 2000°C and the range of the applied fluence was up to 7×10^{25}m^{-2}. The erosion yield we observe exceeds the value expected from physical sputtering data by a factor of 2. In addition we observe an Arrhenius-like increase of the erosion yield with temperature with an activation energy of 0.04 eV.

1. Introduction

Tungsten is considered to be of vital importance for the design of well performing and sufficiently long-lived divertor components for future fusion reactors. In a power reactor divertor there will be a D/T plasma with a concentration of He in the range of 5-10%. Synergistic effects of simultaneous irradiation of tungsten surfaces with He particles and high heat flux were observed for instance in [1, 2]. The formation of surface and near-surface features with typical dimensions in the range of nanometres to micrometres under irradiation with He or H/He mixtures has been reported for tungsten from a number of plasma or high heat flux experiments [3, 4, 5]. The resulting morphology after irradiation with a H/He mixture is distinctly different form the morphology after irradiation with the pure species. The question how this morphology influences the erosion behaviour of tungsten has been addressed in linear plasma devices and also in tokamak edge plasmas [6, 7, 8].

Detailed studies of the morphology development upon irradiation with 30 or 100 keV He ions have recently been reported from electrostatic confinement devices [9, 10, 11].

2. Experimental

We devised a method to measure erosion in the micrometre range on actively cooled tungsten samples exposed to a H/He beam in the high heat flux device GLADIS [12]. A detailed description of the method and analysis tools as well as the original publication of the erosion data can be found in [13].

The method is based on engraving markers by using a focused ion beam onto the side surfaces of our samples prior to joining them to the heat sink. SEM analysis of the marker position

with respect to the sample surface before and after exposure allows us to measure directly the amount of eroded material. With this method we have investigated the erosion of tungsten exposed to a mixed beam of 94% H and 6% He at a power density of 9 MW/m² to 10.5 MW/m² and a particle flux density of $3.1\text{-}3.7\times10^{21}\text{m}^{-2}\text{s}^{-1}$. The variation of these parameters originates from the Gaussian distribution of the beam profile. The employed acceleration voltage was 28 kV. The hydrogen atomic flux consists of 22% H from H^+, 43% from H^{2+} and 35% from H^{3+}. We investigated samples at stationary surface temperatures of 600°C, 1000°C, 1500°C, and 2000°C in a fluence range of 1.7×10^{25} m^{-2} to 6.9×10^{25} m^{-2}.

The base pressure of the GLADIS vacuum vessel is below 10^{-7} mbar. During the high heat flux pulse the pressure rises up to 2×10^{-3} mbar H/He due to the gas injection into the beam source. Oxidation of the sample surfaces is therefore not considered to be a problem.

3. Results

3.1 Erosion data analysis

Here we present a comparison of the data with predictions from physical sputtering and an analysis of a possible temperature dependent trend of the erosion behaviour.

The amount of eroded material was measured using focused ion beam preparation and scanning electron microscopy. The erosion data are shown in figure 1 in four panels a) to d) together with error bars in micrometres versus the incident fluence. These data are measured directly on the samples by analysing the distance of markers on a side face from the top surface before exposure and after applying the respective fluence. The accuracy of this analysis is in the range of a few hundred nanometres. During the loading the higher temperature samples show substantial grain growth from initially a few microns typical size to about 60 microns after loading for one hour at 1500°C or 2000°C [14]. For such a grain size our method analyses the erosion behaviour of one individual grain only. The investigation by confocal scanning laser microscopy, however, shows that each grain has an individual height and therefore an individual amount of erosion, since the initial sample surfaces were polished flat. Therefore we analysed the surface topography on each sample in an area of 640 µm × 640 µm and computed the respective standard deviation, which is in the range of 0.5 µm to about 3 µm. The error bars shown in figure 1 include this standard deviation as well as the error from the individual erosion measurement for each sample.

All panels in figure 1 additionally show a dashed line. This represents the erosion expected from physical sputtering computed for the species and energy distribution present in the centre of our incident GLADIS beam based on published data [15] for normal incidence on flat surfaces. The first conclusion that can be drawn from the data presented in figure 1 is therefore the observation that the measured erosion exceeds the one expected from physical sputtering for all investigated temperatures and fluences.

In addition, the data in figure 1 show a systematic increase of the slope with increasing temperature, i.e. from panel a) to panel d). Therefore the possibility of a temperature dependence of the erosion yield is analysed in the following.

The error bars we introduced are not solely based on the statistics of the erosion measurement itself. In addition we do not know a priori how well our measured data would fit into a statistical distribution of erosion data, i. e. we must assume that we have outlier data points in our results. The usual least squares procedure is known to be very sensitive to outliers. Therefore we analysed the slopes of our data using a method which is more robust to statistical outlier data points than the least squares method: As recommended in "Numerical Recipes" a simple robust estimate can be obtained by minimizing the sum of the absolute deviations instead of the squares [16]. Since we know that at zero fluence we have zero erosion we have as a model assumption:

$$Y = \boldsymbol{a} \cdot X \qquad (1)$$

with Y being the erosion and X the fluence and $\boldsymbol{a}$ the slope we want to determine, i.e. the erosion yield. We determine $\boldsymbol{a}$ by minimizing the sum of the absolute deviations weighted by their individual error bars σ_i:

$$\min_{\boldsymbol{a}} \sum_i \frac{|Y_i - \boldsymbol{a} \cdot X_i|}{\sigma_i} \qquad (2)$$

This procedure results in a systematic increase of the erosion yield from 7.2×10^{-3} at 600°C to 9.7×10^{-3} at 2000°C. The value obtained from physical sputtering data published in [15] (see fig. 1)) is 4.1×10^{-3} and is assumed to be independent of temperature. The solid lines in figure 1 represent the resulting erosion using equation (1). The dashed lines represent the above erosion from physical sputtering data, which is assumed to be temperature-independent.

To test whether the observed temperature dependence is based on a thermally activated process, we have plotted the resulting erosion yields versus the inverse temperature in an Arrhenius plot. This is shown in figure 2. The open circles represent the yields we obtain from the procedure described above, while the crosses result from a least squares minimizing procedure. Comparing these two types of analyses it can be seen that the resulting yields coincide except for the 2000°C data. The solid line in figure 2 represents a fit to the open circles, i.e. to the robust estimate yields. It must be concluded that the data are well represented by a straight line in the Arrhenius plot, which gives a strong indication for the presence of a thermally activated mechanism in the erosion process. The activation energy we deduce for this process from our analysis is 0.04 eV.

Summarizing the findings presented in this section, we conclude that the observed erosion exceeds the value expected from physical sputtering in all investigated cases. Additionally, the observed erosion yield increases systematically with temperature in an Arrhenius dependence by about 35 % from 600°C to 2000°C.

3.2 Investigation of possible mechanisms

The analysis of the erosion data presented in section 3.1 clearly shows that the observed amount of erosion exceeds the value predicted from physical sputtering data by roughly a factor of 2. In addition, the data suggest the presence of a thermally activated mechanism in the erosion process.

Several possibilities are conceivable for this deviation from the prediction based on physical sputtering modelling. In the following we investigate two of these possible causes. The most obvious is the formation of a distorted surface layer, as shown in several experiments (see references [1-11]), which is investigated as a function of fluence and temperature in section 3.2.1. The second is the dependence of the sputtering yield on the crystal orientation. To investigate this, section 3.2.2 presents results from a crystallographic texture analysis.

3.2.1 Cross-sections

Figure 3 shows cross sections prepared by focussed ion beam for the samples with the highest fluences for all four surface temperatures. All shown cross sections were imaged with identical magnification. The observed features change systematically with increasing temperature. While at 600°C the only observable features look like localized cleavage fracture, there are distinct cavities present in the subsurface region at the higher temperatures. It is presently not clear whether these cavities are gas filled or not. The cavity size distribution for 1500°C and 2000°C has been analysed in [14]. It was found that for 1500°C the size distribution is bimodal with one maximum at 50 nm and another one at 200 nm. For 2000°C the number of large cavities decreases while there appears to be an increased number of smaller cavities.

To obtain a further quantitative statement we analysed the thickness of the surface layer affected by the formation of cavities. This was performed for all four temperatures for the samples which had experienced the highest and lowest fluences, respectively. The measured parameter was the vertical distance from the surface to the deepest-lying resolvable cavity for a fixed resolution. The analysis consisted of 25 to 150 individual depth measurements depending on the respective sample. The results are shown in figure 4. The error bars shown in the figure are standard deviations computed from the respective ensemble of measurements.

The result for the 600°C sample is distinctly different from the other three temperatures: Figure 4 also shows the projected range of 28 keV H (solid horizontal line) and of 28 keV He (dashed horizontal line) in tungsten taken from ref [17]. TRIM-based values published in a recent report [18] are larger by 30% to 80%. Within the error bars the observable localized cleavage features in the 600°C samples are in the projected range of H implantation for a fluence of 2×10^{25} m^{-2} as well as for $6\times10^{25}m^{-2}$. For the other three surface temperatures there is a distinct jump exceeding the projected range by a factor of 4. Obviously there is a threshold temperature for the onset of cavity formation, which must be in between 600°C and 1000°C. Otherwise there is no variation of the affected layer thickness observable. The three data points coincide at the lowest fluence and within the error bars there is no further change with fluence in the investigated range.

3.2.2 Crystallographic texture

References [19, 20] report an orientation dependence of the sputtering yield for the bcc metals molybdenum and tungsten. In both cases the (110) crystal plane, i.e. the face diagonal of the

unit cell, shows the highest yield during sputtering with Ar at 5 keV and 0.6 keV, respectively. For this reason we analyzed our samples by X-ray diffraction to investigate the presence of texture, i.e. a preferential crystal orientation on the sample surface. The information depth for X-ray diffraction depends on the specific reflex angle but is generally in the range of not more than a few µm for the used copper K_α radiation in tungsten.

A (110) fibre texture was found on all samples exposed to 1500°C and 2000°C. "Fibre texture" means that the sample surfaces have a prefererential crystal orientation with the (110) crystal plane parallel to the loading surface while there is no specific preferred orientation in any other direction. The samples exposed to 600°C and 1000°C, respectively, did not show this texture. This is presumably due to the fact that the samples were cut out of rods in different orientations.

4. Discussion

Generally it is assumed in the literature that physical sputtering by particle bombardment is insensitive to the target temperature [21]. In section 3.1 we present erosion yields which are higher than expected from physical sputtering data and additionally show a distinct temperature dependence. The possible origin of these two features is discussed in the following in the frame of the additional information we presented in section 3.2.

In reference [19] a factor of about 1.5 is found in between the sputtering yield of a molybdenum (110)-surface and a molybdenum (100)-surface upon irradiation with 5 keV Ar. The data in reference [20] indicate an increase of the sputtering yield between the polycrystalline average and the (110) crystal orientation of up to 10% when sputtering with 0.6 keV Ar. These observations can be understood qualitatively since the (110) planes in a bcc metal are the ones with the highest atomic plane distance [22].

Based on these facts the presence of a 110 fibre texture on our 1500°C and 2000°C samples could qualitatively account for the difference observed between the high-temperature (1500°C and 2000°C) and the low-temperature samples (600°C and 1000°C). It is unclear whether the 35% increase of the erosion yield from 7.2×10^{-3} at 600°C to 9.7×10^{-3} at 2000°C can be fully accounted for by the formation of the 110 fibre texture. The fact that all samples have an erosion yield higher than predicted from physical sputtering data cannot be accounted for.

In [22] a dependence of the sputtering yield on the degree of crystallinity is mentioned, since channelling can effectively reduce the sputtering yield. This motivates the investigation of the temperature and fluence dependence of the thickness and morphology of the distorted subsurface layer. As figures 3 and 4 show clearly, we find a distinct jump in the formation of cavities and the thickness of the affected layer between 600°C and 1000°C. From 1000°C to 2000°C we find no distinct influence of the surface temperature or the fluence on the thickness of the affected layer within the error bars, although there is a trend visible for the high fluence data, which does, however, not exceed the error bars.

The thickness of the layer affected by cavity formation is shown in figure 4 to be fluence independent. Similar to the model for fuzz layer thickness described in [23] a fluence-independent constant thickness of the affected layer can be expected based on a dynamic

equilibrium between growth and erosion. In the much lower fluence range below 10^{20} m^{-2} reference [9] reports a clear fluence dependence of the affected layer thickness.

If we assume that the growth of the affected layer is connected to diffusion of helium, then the diffusion activation energy of helium in tungsten is possibly involved, which is given as 0.06 eV in reference [24]. As we observe an increase of the erosion yield with an activation energy of 0.04 eV, there is the possibility that the temperature dependencies of these two processes are similar, which would result in a constant affected layer thickness independent of fluence and temperature.

5. Summary and outlook

We devised a method for the direct measurement of tungsten erosion on actively cooled samples upon irradiation with a mixed H/He beam in GLADIS, which is based on focused ion beam preparation of markers. We have measured the erosion yield for fluences up to 7×10^{25} m^{-2} at stationary surface temperatures varying from 600°C to 2000°C and found an amount of erosion in excess of physical sputtering predictions as well as an Arrhenius-like increase of the erosion yield.

To investigate possible causes we examined the texture as well as the fluence and temperature dependence of the morphology formation. We have identified the presence of a (110) fibre texture on some samples, which may affect the erosion yield. However, this cannot account for the excess erosion we observe for all investigated samples as compared to physical sputtering data and it cannot explain the Arrhenius-like temperature dependence we observe. Also the analysis of the morphology development with fluence and temperature does not yield an explanation for the observed erosion behaviour.

Experiments with varying helium concentrations in the beam as well as H/He retention studies by thermal desorption are in progress.

Figures

Figure 1: Linear plots of eroded amount of tungsten in micrometres versus incident particle fluence in 10^{25} m^{-2} for surface temperatures of a) 600°C, b) 1000°C, c) 1500°C, and d) 2000°C. The black solid lines are based on the erosion yields determined according to equations (1) and (2). The dotted lines represent the erosion based on physical sputtering data.

Figure 2: Arrhenius plot of the erosion yields for all four temperatures. Open circles are based on the robust estimate minimization of absolute deviations (equations (1) and (2)), crosses are based on a least squares minimization. The solid line is a fit to the robust estimate data yielding an activation energy of 0.04 eV. The dashed line is a fit to the least squares data, which yields 0.03 eV.

Figure 3: SEM images of focused ion beam cross-sections of the samples exposed to the highest fluence for all four temperatures. All images are in identical magnification. The vertical stripes are artefacts due to the FIB preparation.

Figure 4: Layer thickness of the subsurface range affected by cavity formation for samples exposed to the lowest and highest fluences, respectively. Error bars are standard deviations. The solid and dashed horizontal lines are projected ranges for 28 keV H and He, respectively, based on reference [17].

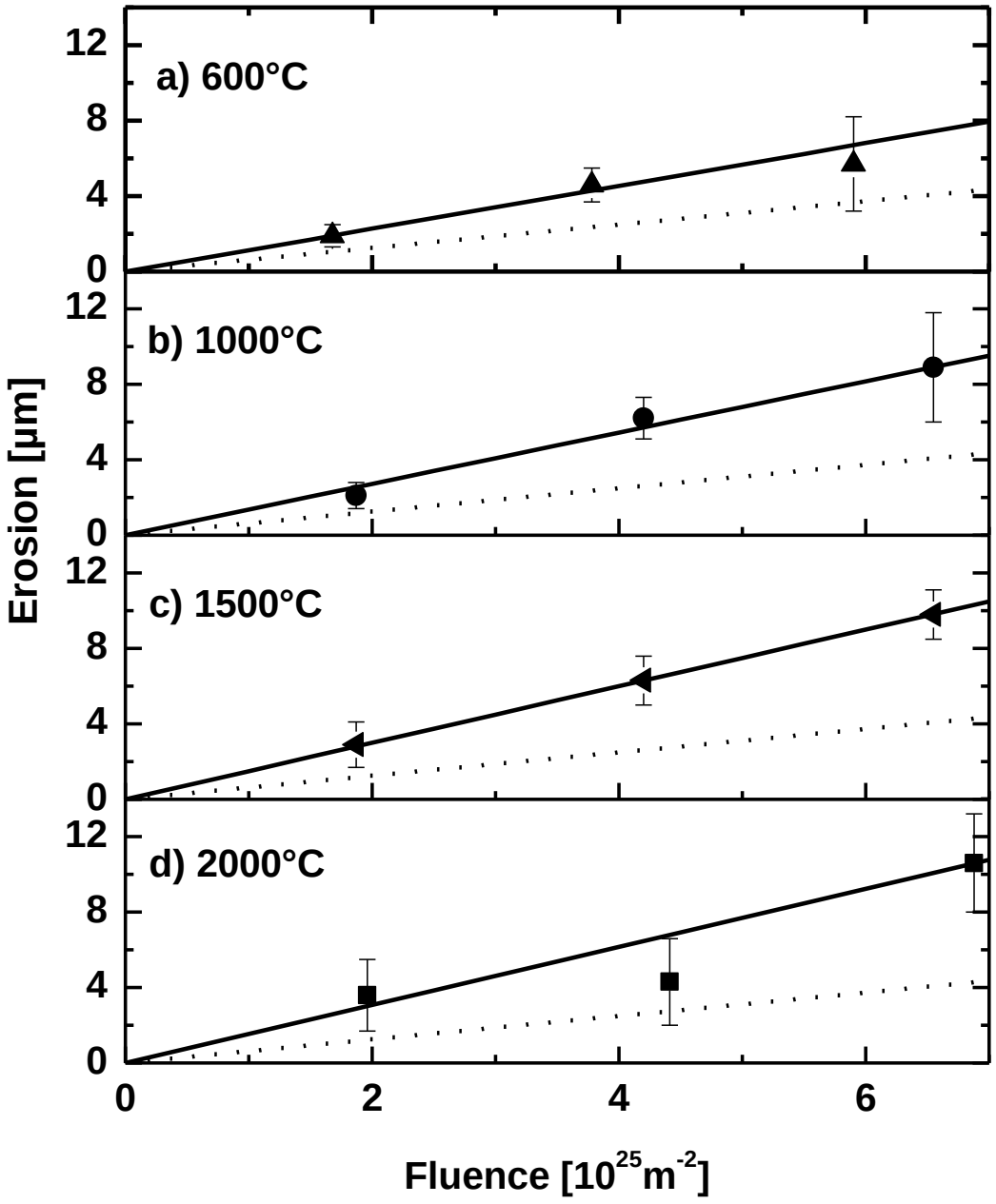

Figure 1 (single column)

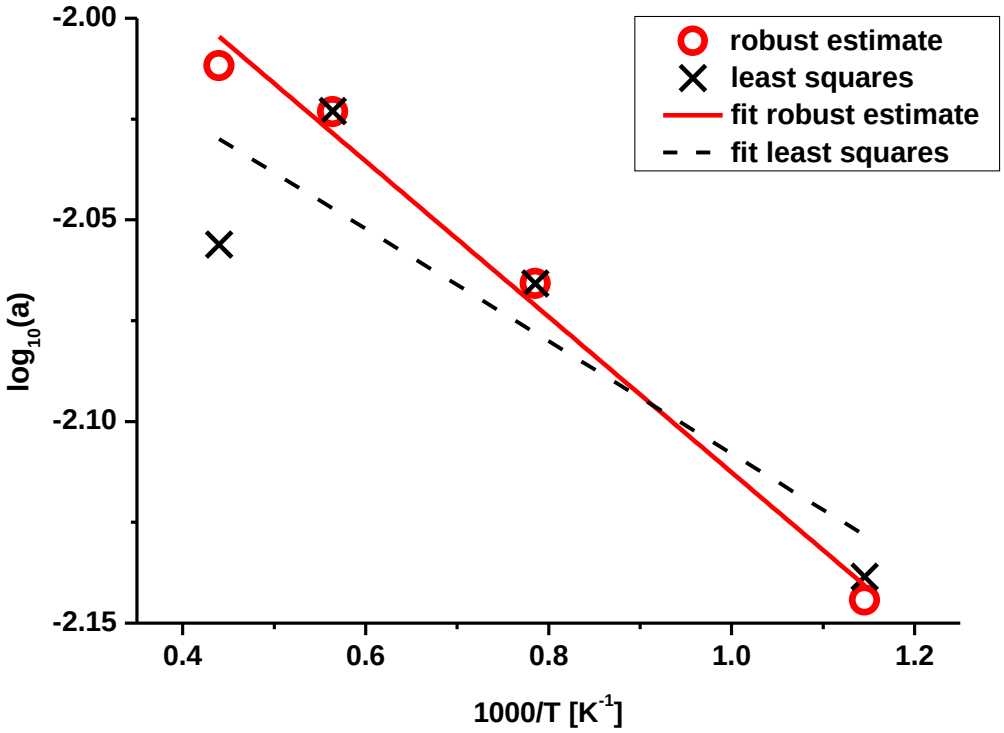

Figure 2 (single column)

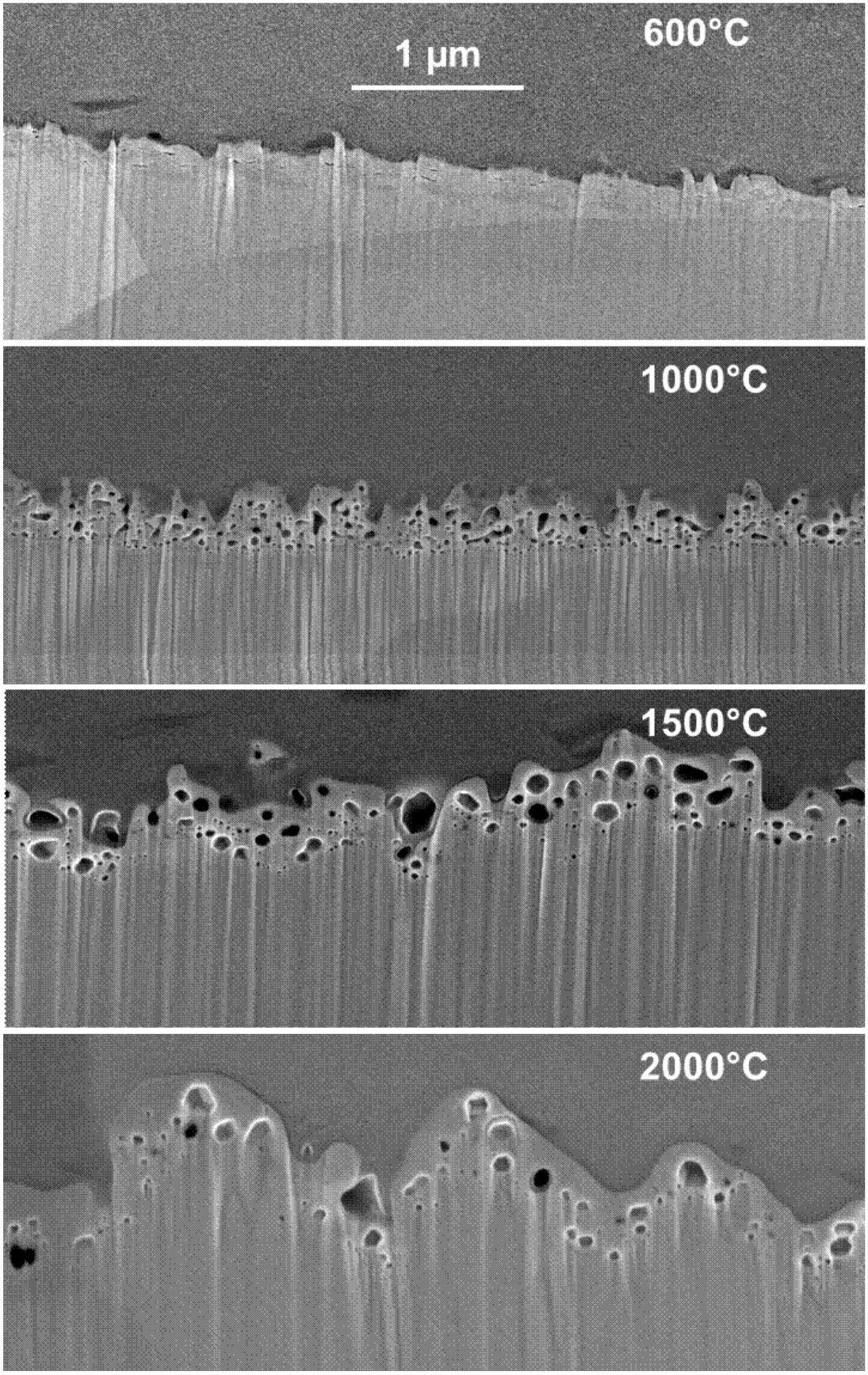

Figure 3 (single column)

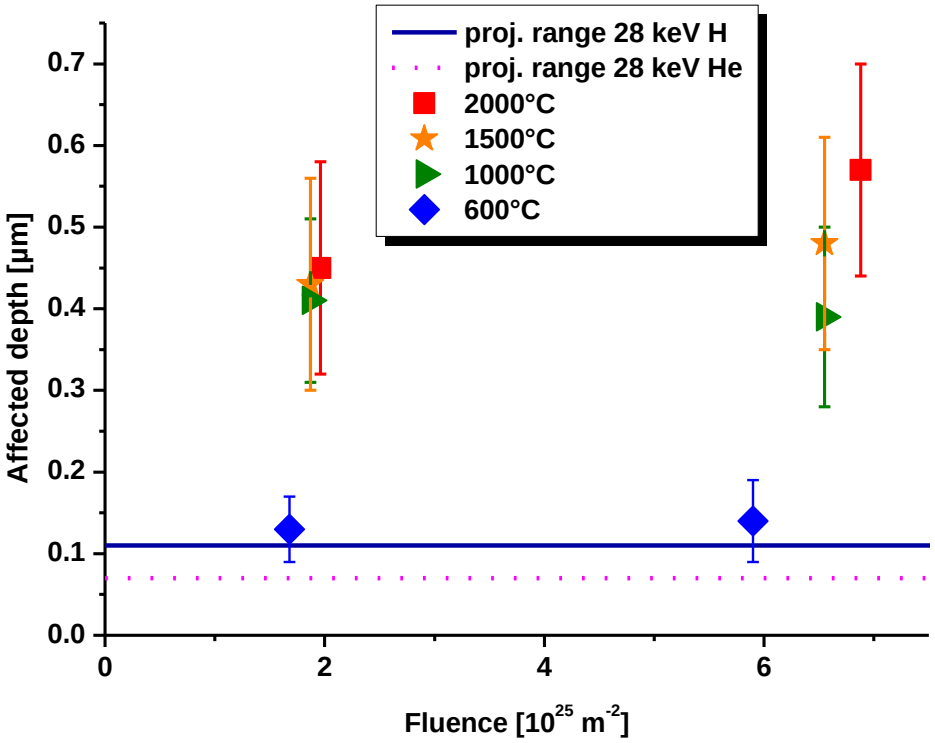

Figure 4 (single column)

References

1 K. Tokunaga et al., J. Nucl. Mater. 329-333 (2004) 757

2 K. Tokunaga et al.,, J. Nucl. Mater. 390-391 (2009) 916

3 M.J. Baldwin, R.P. Doerner, Nucl. Fusion 48 (2008) 035001

4 S. Kajita et al., Nucl. Fusion 49 (2009) 095005

5 H. Greuner et al., J. Nucl. Mater. 417 (2011) 495

6 D. Nishijima et al., J. Nucl. Mater. 415 (2011) S96

7 S. Kajita et al., Plasma Fusion Res. 4 (2009) 004

8 Y. Ueda et al., J. Nucl. Mater. 415 (2011) S92

9 S. Zenobia, L. Garrison, G. Kulcinski, J. Nucl. Mater. 425 (2012) 83

10 S. Semsari et al., J. Fusion Energ. 31 (2012) 389

11 S. Semsari et al., J. Fusion Energ. 32 (2013) 142

12 H. Greuner et al., J. Nucl. Mater. 367-370 (2007) 1444

13 H. Maier et al., J. Nucl. Mater. 438 (2013) S921

14 H. Greuner et al., J. Nucl. Mater. (2013) Investigation of European tungsten materials exposed to high heat flux H/He neutral beams, DOI: 10.1016/j.jnucmat.2013.04.044

15 R. Behrisch and W. Eckstein (eds.), „Sputtering by particle Bombardment", Topics in applied physics 110, Springer, Berlin/Heidelberg 2007

16 W. H. Press et al. (eds.), Numerical recipes: The art of scientific computing, third edition, section 15.7, Cambridge University Press 2007

17 M. J. Berger et al., Stopping-Power and Range Tables for Electrons, Protons, and Helium Ions, http://www.nist.gov/pml/data/star/index.cfm

18 W. Eckstein, IPP Report „Penetration (Range)", IPP 17/20, Max-Planck-Institut für Plasmaphysik, Garching 2010

19 C. E. Carlston et al., Phys. Rev. 138 (1965) 759

20 V.S. Voitsenya et al., J. Nucl. Mater. 434 (2013) 375

21 P. Sigmund and M. Szymonski, Appl. Phys. A 33 (1984) 141

22 H. E. Roosendaal in: Behrisch R. (ed.), „Sputtering by Particle Bombardment I", Topics in Applied Physics 47, Springer Berlin/Heidelberg 1981 (section 5)

23 R. P. Doerner, M. J. Baldwin and P.C. Stangeby, Nucl. Fusion 51 (2011) 043001

24 C. Becquart and C. Domain, Phys. Rev. Lett. 97 (2006) 196402